Special Issue on "Theoretical and Computational Chemistry"

J. Indian Chem. Soc.,
Vol. 96, July 2019, pp. 741-751

Importance of translational jump in diffusion of hydrophobic solute in supercooled water: Solute size dependence

Vikas Dubey, Shivam Dueby†, Shakkira Erimban† and Snehasis Daschakraborty*

Department of Chemistry, Indian Institute of Technology Patna, Patna-801 106, Bihar, India

E-mail: snehasis@iitp.ac.in

Manuscript received online 02 April 2019, revised and accepted 27 April 2019

It has been reported in many experimental and simulation studies that small solutes – dissolved in supercooled water (or supercooled liquid in general) – violates the Stokes-Einstein equation (SE), a hydrodynamic relation connecting the self-diffusion coefficient of the solute, the viscosity of the solvent, the radius of the solute, and the temperature of the system. However, with the increase in the solute's size, the validity of the SE equation is gradually attained. It is generally believed that the presence of translational jump occurrence of the small solute in supercooled water is responsible for the SE breakdown. However, a quantitative estimation of the jump contribution for the self-diffusion of a solute is still lacking. Here, we have performed molecular dynamics (MD) simulations for four different nonpolar solutes (with increasing solute size), separately dissolved in water. By adopting a recent technique for direct identification of translational jump occurrence of the solute molecule, we have successfully calculated the jump-diffusion coefficient of the solute and its contribution to the total self-diffusion of the solute molecule in liquid water both at room temperature and supercooled regime. As the solute size decreases, the contribution of jump-diffusion increases at the supercooled regime. We have also separated the jump-diffusion from the total diffusion of the solute to obtain the residual diffusion, which better follows the SE equation. This is direct evidence for the increased importance of translational jump-diffusion for the observed breakdown of the SE relation for small solutes at the supercooled regime. These new findings can assist in comprehending many experimental results where the breakdown of the SE equation is observed.

Keywords: Supercooled water, molecular dynamics, hydrophobic solute, Jump-diffusion.

1. Introduction

Supercooled water (water below its freezing point) is a fascinating liquid with a large number of anomalous properties. The increasing violation of the Stokes-Einstein (SE) equation, $D = k_BT/6\pi\eta r$, connecting the translational diffusion coefficient D and medium viscosity η, with lowering temperature is one of them[1–4]. The above breakdown starts showing up below $T \sim 2.1T_g$ for water, while for molecular glass forming liquid the SE breakdown is prominent only below $T \sim 1.2T_g$[4]. Similar to the self-diffusion of the liquid molecules, the translational diffusion of a tracer in liquid also violates the SE equation, connecting D with the viscosity η of the liquid medium[5–14].

Many possible ways are available to quantify the extent of violation of the SE equation. Experimental and simulation works generally study the coupling/decoupling of D of the tagged particle from η of the medium instead of direct verification of the SE equation[4]. Sometimes, due to unavailability of accurate viscosity data, structural relaxation time (average translational relaxation time) acts as a proxy based on the fact that the structural relaxation time is generally proportional to the viscosity of the medium[2].

There are many explanations for the above decoupling of the translational diffusion of the tagged particle from the viscosity of the medium at the supercooled regime. The gradual increase of the microscopic spatiotemporal heterogeneity with cooling down the liquid is one of the key reasons[7,8,15–30]. The decoupling is also explained from the second liquid-liquid critical point and the position of the Widom line. Jump translation of a tagged particle in a supercooled

†Both the authors contributed equally.

liquid is a crucial factor for the observed decoupling between the translational diffusion and the viscosity[28]. Goldstein put forward a theory on the temperature dependent mechanism of translational diffusion of liquid molecules[18,24,31–38]. The theory suggests that while at the low temperature a tagged particle in the liquid diffuse via large step jump from one saddle point to another in the rugged free energy landscape, the particle translates via small step Brownian motion at a higher temperature. Several theoretical and computer simulation studies confirmed the characteristics of this picture[18,24,31–38].

A recent study by two of us has successfully calculated – for the first time using the radius of gyration method – the jump-diffusion coefficient D_J of the water molecules at a wide range of temperatures including the deeply supercooled regime[39]. The above study has addressed the increasing importance of translational jump diffusion of the water molecules in the diffusion-viscosity decoupling with decreasing temperature. By separating D_J from the overall diffusion coefficient D the residual diffusion coefficient D_{Res} is obtained. D_{Res} remains strongly coupled with the viscosity at the studied temperature range.

The present work focusses on the effect of solute size on jump-diffusion coefficient of the solute molecule in supercooled water. It was observed earlier that the solute's diffusion gets increasingly decoupled from the medium viscosity as the solute/solvent molecular size ratio decreases[40]. For the diffusion of Lennard-Jones (LJ) solute in LJ solvent, three different regimes were identified based on the diffusivity of the solute with variable sizes. The validity of the SE equation is evidenced when the solute/solvent size ratio is higher than ~0.5. The "small solute" regime was seen for solute/size ratio less than ~0.17. In the intermediate regime, where the diffusivity of the solute is very high, it is termed as the "levitation effect".

Even though the above studies have suggested the importance of translational jump-diffusion of a small solute for the breakdown of the SE relation in supercooled water (liquid), more direct and quantitative estimation of D_J is still missing. The present work is an MD simulation attempt for the direct evaluation of D_J of four different hydrophobic solutes in water and prediction of the percentage contribution of D_J to the overall diffusion of the water molecules D.

This study provides insight into the role of the translational jump-diffusion of the solute molecules for the increasing breakdown of the SE relation with decreasing the solute size at the supercooled regime. Moreover, the exploration of the jump-diffusion of the hydrophobic solute in supercooled water is also important in cold denaturation of the protein. Enhanced fluctuation of some protein domains, which has been witnessed at low temperature, plays a vital role for cold denaturation of the protein[41]. It is interesting to note that high fluctuating domains are generally localized within the protein core regions. It is well known that the water-soluble proteins have a hydrophobic core, in which side chains are buried from water, which stabilizes the folded state[42,43].

The organization of the rest of the paper is as follows. In Section 2 we describe the simulation protocol and the force-field parameters of the molecules. Results and discussions are detailed in Section 3. Section 4 summarizes the results and offer concluding remarks.

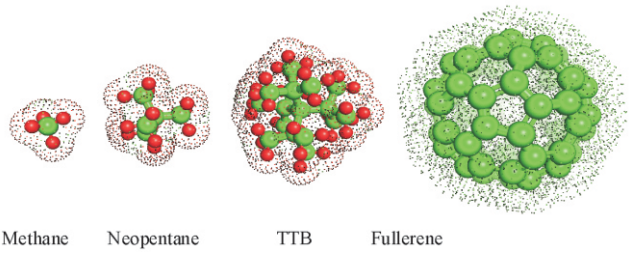

Scheme 1. Molecular structures of the four hydrophobic solutes arranged in order of increasing size from left to right.

2. Simulation details

We have used GROMACS package[44] for performing the MD simulation. The system includes 2000 water molecules and a solute molecule. We have considered four different hydrophobic solutes: methane, neopentane, tetra-*tert*-butylmethane (TTB), and fullerene. The structures of the molecules are presented in Scheme 1. The initial system is built using Packmol software[45]. The above choice of solutes provides a range of solute radius from ~2.0 Å to ~6.0 Å. The solutes are modeled by OPLS/AA force field[46] while water molecules are modeled byTIP4P/2005 force field[47]. It was observed that the OPLS/AA force fields for methane[48], neopentane[49], and fullerene[50] works reasonably well. For

TTB, we have not found any literature work on MD simulation study. TIP4P/2005 water model has proven efficacy in predicting various experimental structural and dynamical properties of water at a wide range of temperatures including deeply supercooled regime.

Simulations are carried out at two different temperatures, 240 K and 300 K. Since the freezing temperature of TIP4P/2005 water is 252 K at 1 atm pressure, 240 K temperature represents the supercooled regime. Therefore, this study focuses on the dynamics of the solutes in water at room temperature and in the supercooled regime. We have maintained the pressure at 1 bar for both the temperatures throughout the simulations. First, we use the steepest-descent algorithm for classical energy minimization of the systems. The classically energy minimized configuration is then equilibrated for 50 ns time using NPT ensemble, during which the temperature is kept constant at the respective desired temperatures using the Nosé-Hoover thermostat[51,52] and maintained pressure using the Parrinello-Rahman barostat[53]. The final box length is presented in Table 1. We have chosen 0.5 ps and 1 ps for the pressure and temperature coupling constant respectively. Further, we have performed production runs of 1 μs for 240 K and 500 ns for 300 K for each of the solutes using NPT ensemble. These simulations sums to a total of 6 μs long simulation.

We have used the Leapfrog-Verlet algorithm for solving the equations of motions with a time step of 2 fs. The production trajectory is saved at a regular interval of 100 fs. A cut-off distance of around half of the box length is applied for LJ interactions. Particle Mesh Ewald summation technique is used to handle the long-range Coulomb interactions. During the simulations, all the bonds are constrained with LINCS algorithm[54].

Table 1. The average box lengths for the systems at two different temperatures

System	Box length (Å)	
	T = 240 K	T = 300 K
Methane	39.32	39.17
Neopentane	39.33	39.19
TTB	39.37	39.24
Fullerene	39.42	39.29

3. Results and discussion

3.1. Hydration structure

We first study the hydration structure (both the spatial and orientational) around the different hydrophobic solutes. We calculate the radial distribution functions ($g(r)$) between the center-of-mass (COM) of the solute and solvent water O_W. Fig. 1 exhibits the $g(r)$ plots for four different solutes at two temperatures. As expected, the $g(r)$ peaks shift towards higher r values with increasing the solute size. More interestingly, for the alkanes, the first peak intensity decreases with increasing the hydrophobic solute size. This is as per earlier simulations, where a similar reduction of first peak height was observed on increasing the size of the methane cluster[55]. The above reduction is supposedly due to a gradual dewetting transition. However, for fullerene, the intensity of the first peak of $g(r)$ is higher than those for the other alkanes. The current simulated $g(r)$ is in good agreement with earlier simulated $g(r)$[56]. The greater intensity of the fullerene-

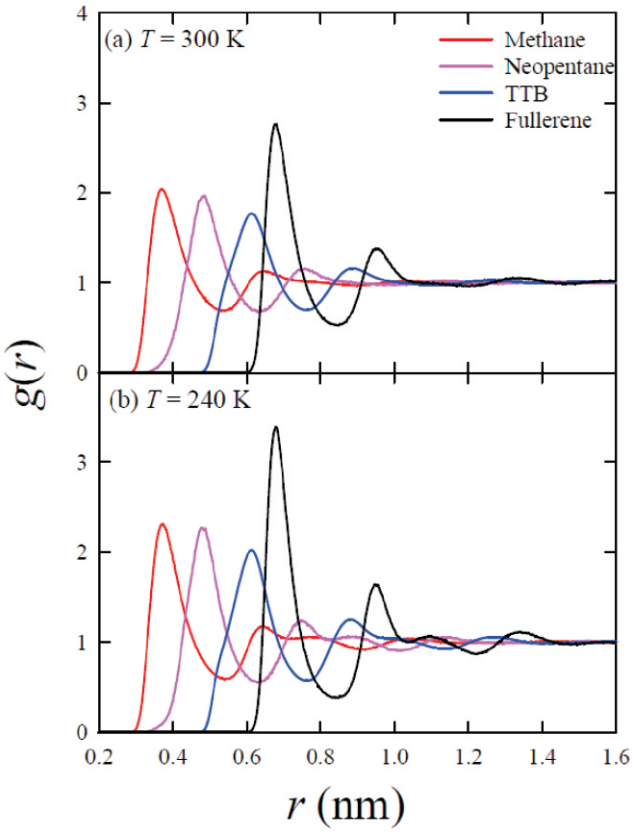

Fig. 1. Radial distribution functions between the COM of the four different solute molecules and water O_w atoms at the temperatures: 300 K (a) and 240 K (b).

water $g(r)$ peak compared to the alkane-water $g(r)$ peak may be due to the difference of shape factor. While C60 is perfectly spherical, the alkanes are having tetrahedral geometry. Therefore, the hydration structure around C60 is more spherical and regular compared to that around the alkanes. This is also suggested by the larger width of the alkane-water $g(r)$ compared to that of the C60-water $g(r)$.

The $g(r)$ peaks at long distance r are clearly visible beyond the second peak for T = 240 K, while they are not visible at 300 K temperature. These long distance peaks are probably emanating from the collective structural ordering (lowering of entropy) of supercooled water molecules. A recent study[57] has already focussed on the temperature-dependence of water-water $g(r)$ at higher r. This study has indicated the possible HDL-LDL transition as a possible origin of the $g(r)$ peaks at longer r.

We now present the angular structure of the solvent water molecules around the hydrophobic solutes. Fig. 2 presents $P(r,\theta)$, which is a two-dimensional probability density distribution of the angle θ – between water $O_W\cdots$solute COM vector and the water O_W-H_W bond vector – and the distance r between water O_W atom and the solute's COM at T = 240 K for four different solutes (Similar pictures are obtained for T = 300 K but not shown here). It is evident from Fig. 2 that the

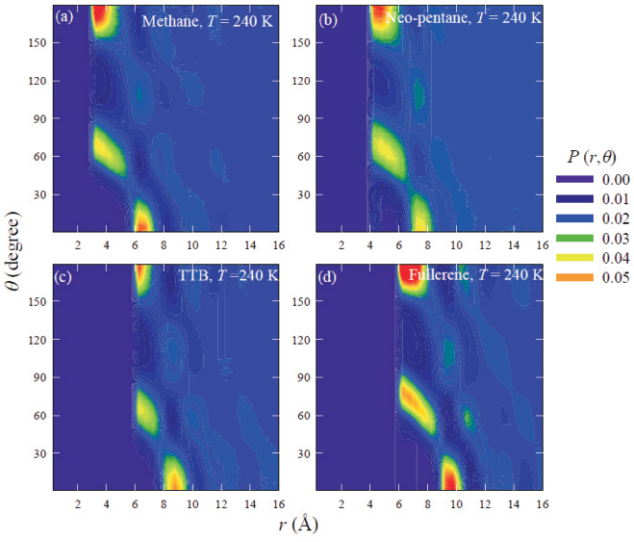

Fig. 2. Two-dimensional probability density distribution, $P(r,\theta)$, of the angle θ – between water $O_W\cdots$solute COM vector and the water O_W-H_W bond vector – and the distance r between water O_W atom and the solute's COM at T = 240 K for four different solutes.

water molecules at the interface of the hydrophobic solute are oriented in a particular fashion. Either the water molecules are oriented tangential with the solute surface (tangential OH with $\theta \sim 65^o$), or they are aligned towards the bulk water (bulk OH with $\theta \sim 180^o$). No dangling OH bonds are found near the solute (dangling OH with $\theta \sim 0^o$), which confirms the absence of H-bonds between the solute and the solvent water molecules. The peaks – situated at the second hydration shell positions – indicate that the majority of the second shell solvent water OH bonds are aligned towards the solute such that these water molecules form H-bonds with the interfacial water solvent molecules. The above orientational order is almost invariant to the solute size and temperature, except slight changes of the peak intensity. The above hydration structures of the four solutes confirm the hydrophobicity of the solutes in TIP4P/2005 water solvent[58–69].

3.2. Diffusion of the solutes: Size dependence

We calculate self-diffusion coefficient D of the solute molecules dissolved in water at two different temperatures using the mean square displacement (MSD) route. MSD is calculated using the equation, $\langle|\Delta r(t)|^2\rangle = \langle|r_i(t) - r_i(0)|^2\rangle$. Here, $r(t)$ and $r(0)$ are the positions of the solute molecule at time t and time t = 0 respectively. Fig. 3 presents MSDs against time for four different solutes, each at two temperatures. In all cases, MSDs show three distinct regions: (i) the ballistic part ($\langle|\Delta r(t)|^2\rangle \alpha\ t^2$) at short time, (ii) the diffusive part ($(\langle|\Delta r(t)|^2\rangle \alpha\ t)$) at the longer time, and (iii) the sub-diffusive part at intermediate time ($\langle|\Delta r(t)|^2\rangle \alpha\ t^{\alpha}$; $0 < \alpha < 1$). This sub-diffusive part of MSD appears from the rattling motion of the solute molecule, which is momentarily trapped inside the solvent's cage[24,38,39,70–77]. At room temperature, the sub-diffusive regime is more prominent at an intermediate time for the methane solute. The above region decreases with the increase of the solute size. For fullerene, this regime is almost invisible. However, at T = 240 K, the sub-diffusive part is much more intense for all the solutes. This indicates that the trapping of a hydrophobic solute in supercooled water solvent cage is significant irrespective of the solute's size, while at room temperature the trapping is mainly important for small hydrophobic solutes[24,38,39,70–77]. D is calculated by fitting the MSDs of the solutes at diffusive limit using the following equation, $\langle|\Delta r(t)|^2\rangle = 6Dt$.

Table 2 lists the D values of the solutes at two temperatures. Clearly, at both the temperatures, the D value de-

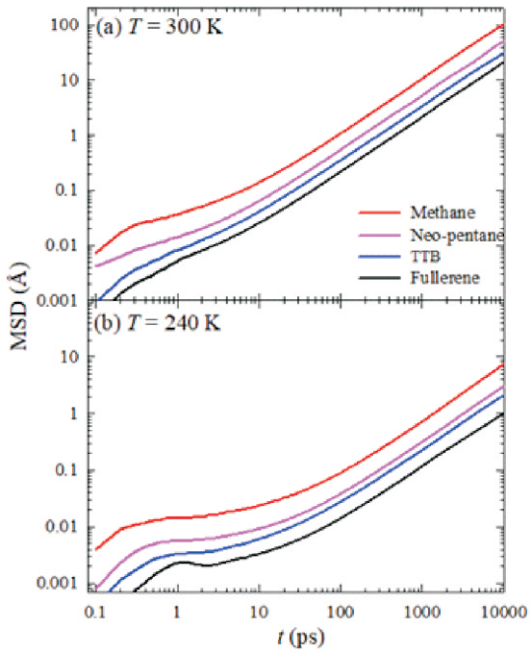

Fig. 3. Mean square displacement of the solute molecules as functions of time at the two temperatures, 300 K (a) and 240 K (b).

creases with increasing solute's size. The solutes diameters have been determined using the following equation, $\sigma_S = 2(r^1_{S-W} - r^1_{W-W})$, where r^1_{S-W} and r^1_{W-W} are the 1st peak position of the $g(r)$ between the solute and water O_W and the 1st peak position of the water O_W-water O_W $g(r)$. σ_S values of the solutes are listed in Table 2. Table 2 clearly shows that while the solute's size is decreased by ~2.5 times on replacing the solute fullerene by methane, solute's D value increases by ~10 times at 240 K temperature. This strongly contradicts to the behavior predicted from the SE equation, where D is just inversely proportional to the solute's diameter (that is the increase of D value at the same proportion with the decrease of solute's size). At room temperature, however, the violation of the SE equation is not so intense as the solute's D value increases by ~5 times as the solute's size is decreased by ~2.5 times. The stronger breakdown of the SE equation at 240 K temperature is very similar to the decoupling of diffusion of supercooled liquid from viscosity. We will see in the next section, the importance of the jump translation for the self-diffusion of the small solute in supercooled water.

Table 2. The calculated diameters of the solutes ($\sigma_S = 2(r^1_{S-W} - r^1_{W-W})$), and the total self-diffusion coefficient D of the solutes at two temperatures

System	σ_S (Å)	$D/10^{-5}$ (cm^2/s)	
		T = 240 K	T = 300 K
Methane	4.46	0.124	1.744
Neopentane	6.78	0.046	1.150
TTB	9.38	0.034	0.451
Fullerene	10.66	0.015	0.308

3.3. Calculation of the jump-diffusion coefficient

Now, we turn our focus on estimating the translational jump contribution to the total self-diffusion coefficient of the solutes at two temperatures. Here, the key is to identify a real translational jump occurrence of the solute correctly. Multiple ways are possible for identifying a jump event. The simplest of all is via following over time the displacement of the solute molecule from its position at t = 0 and finding the point when a rapid change of displacement happens[24,38,39,78–80]. This method was only successful in tracing the presence of jump event in the trajectory of the solute molecule and understand the mechanistic pathway of a translational jump event. Unfortunately, being based on manual identification of the jump events, this approach fails in a quantitative analysis of jump-diffusion coefficient.

Another method, based on oscillator model theory[81], was used to calculate the jump-diffusion coefficient (neck diffusion) of a small solute particle in a viscous liquid. This method captured the increased relevance of jump-diffusion of a small solute molecule through solvent cages[82]. However, it is not clear whether the same theory is applicable for estimating the jump-diffusion coefficient of bigger solute and solvent molecules.

We have used here a different method, previously developed by Raptis *et al.*[83,84] and later modified by Araque *et al.*[85]. This method has been recently used by three of us for understanding the importance of translation jump of supercooled water molecules for increasing decoupling of the self-diffusion coefficient of water from viscosity with decreasing temperature[39]. In this method, we first split the long trajectory of a solute molecule and calculate the radius of gyration R_g for each of the trajectory segments. R_g, for a trajectory segment of length Δt (n time space), is calculated using the following equation[39,83–85],

$$R_g(t, \Delta t) = \sqrt{\frac{1}{n}\sum_{i=1}^{n}[\mathbf{r}_i(t;\Delta t) - \mathbf{r}_{CM}(t;\Delta t)]^2} \quad (1)$$

where $\boldsymbol{r}_i(t;\Delta t)$ and $\boldsymbol{r}_{CM}(t;\Delta t)$ are the position of the solute at *i*-th time frame and the center of mass position of the trajectory segment of length Δt. $\boldsymbol{r}_{CM}(t;\Delta t)$ is calculated by the following equation,

$$\boldsymbol{r}_{CM}(t;\Delta t) = \frac{1}{n}\sum_{i=1}^{n}\boldsymbol{r}_i(t;\Delta t) \quad (2)$$

Consideration of the value of Δt in eqs. (1) and (2) must be done judiciously. It is not recommended to use the same Δt value for different solutes and temperature. Because the diffusion of a solute changes significantly with its size and temperature, the consideration of the same Δt for all conditions may not produce correct results. For example, a trajectory segment of Δt =100 ps duration at 240 K temperature explores much less phase space than that at 300 K. Similar situation arises when trajectory segments of the same length is used for two different solutes. All the above problems can be solved if we consider Δt as the time t^*, at which the non-Gaussian parameter $\alpha_2(t)$ goes maximum. We calculate $\alpha_2(t)$ using the following equation,

$$\alpha_2(t) = 3\langle r^4(t)\rangle/5\langle r^2(t)\rangle^2 - 1 \quad (3)$$

where, $\langle r^2(t)\rangle$ is the MSD and $\langle r^4(t)\rangle = \langle|\boldsymbol{r}_i(t) - \boldsymbol{r}_i(0)|\rangle$. Fig. 4 presents $\alpha_2(t)$ as a function of time for four different solutes, each at two temperatures. The peak intensity of $\alpha_2(t)$ increases with decreasing solute size. This indicates an increase of temporal heterogeneity with decreasing solute size. But, t^* (listed in Table 3) shifts towards higher value as the solute size increases. Now, comparison of $\alpha_2(t)$ plots between T = 240 K and 300 K temperatures reveals that the peak heights for all the solutes at 240 K temperature are higher than those at 300 K temperature. Therefore, Δt time duration increases with increasing temperature and decreasing the solute size.

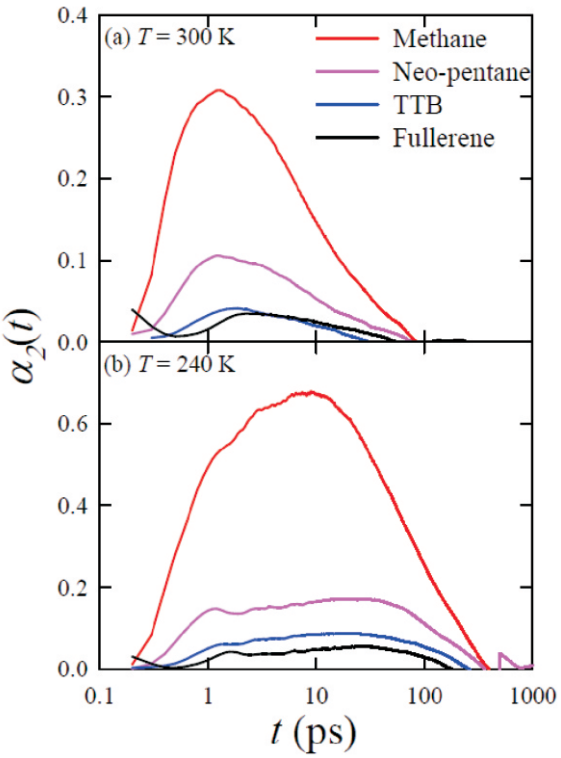

Fig. 4. Non-Gaussian parameter $\alpha_2(t)$ as a function of time for all the solute molecules at the two different temperatures, 300 K (a) and 240 K (b). The time t^* for the maximum value of $\alpha_2(t)$ are listed in Table 3.

As we split the trajectory into segments, each with the duration of Δt time, and we calculate R_g for all these trajectory segments, our next goal is to calculate the distance traversed by the molecule in a trajectory segment $\lambda(t)$. This can be calculated using the equation, $\lambda(t) = 2R_g$[83–85]. Fig. 5

Table 3. Solute size dependence of the time scale t^* (the time when the non-Gaussian parameter $\alpha_2(t)$ is the maximum), the two crossing distances (r_1 and r_2) between simulated and theoretical self-part of the van Hove correlation functions, the number of successful jump occurrences n_J, the jump frequency ν_J, and the average jump length $\langle\lambda_J\rangle$ at two different temperatures

System	T (K)	t^* (ps)	r_1 (nm) Cage	r_2 (nm) Jump	n_J	Jump frequency ν_J (ns^{-1})	$\langle\lambda_J\rangle$ (Å)
Methane	240	9.0	0.11	0.28	2461	2.50	3.27
	300	1.2	0.15	0.41	92	0.18	4.36
Neopentane	240	19	0.08	0.18	740	0.74	2.00
	300	1.2	0.10	0.26	55	0.11	2.72
TTB	240	17	0.08	0.17	19	0.02	1.81
	300	1.8	0.08	0.20	18	0.04	2.09
Fullerene	240	28	0.06	0.14	12	0.01	1.47
	300	2.8	0.08	0.19	10	0.02	1.94

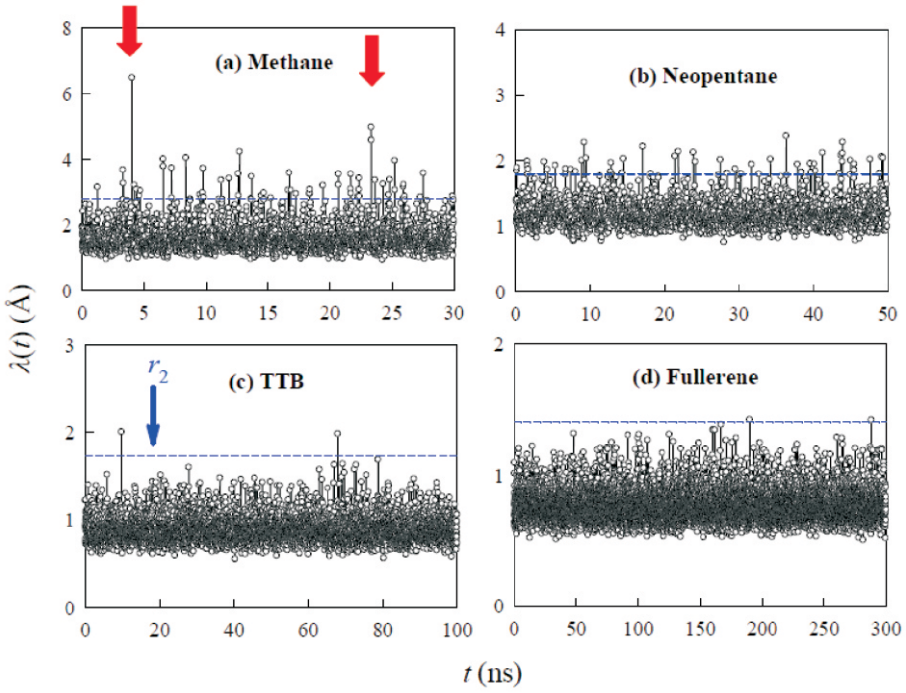

Fig. 5. The plot of λ(*t*) as a function of time for four different solutes at *T* = 240 K temperature. The horizontal lines indicate the cutoff distance r_2, listed in Table 3. The circles, which are above the cutoff distance r_2, represent the jump trajectory segments. The jump trajectory segments for the two λ(*t*) values (indicated by vertical red arrows in panel (a)) are shown by three-dimensional positional phase space in Fig. 7.

plots λ(*t*) as a function of time for all four solutes at *T* = 240 K. Evidently, we have to identify the big successful jumps, which significantly contribute to the jump-diffusion of the solute. For that, we use the self-part of the van Hove correlation function $G_S^{simu}(r, t)$, which can be calculated from the following equation[86,87].

$$G_S^{simu}(r, t) = \frac{1}{N}\left\langle \sum_i^N \delta\left(r - |\mathbf{r}_i(t_0) - \mathbf{r}_i(t)|\right) \right\rangle_{t_0} \qquad (4)$$

It is well known that $G_S^{simu}(r, t)$ deviates maximum from the theoretical Gaussian behavior $G_S^{theo}(r, t) = [3/2\pi\langle r^2(t)\rangle]^{3/2} \exp[-3r^2/2\langle r^2(t)\rangle]^P$ at *t** time, when $\alpha_2(t)$ is maximum (see Fig. 4). We have plotted both the $G_S^{simu}(r, t)$ and $G_S^{theo}(r, t)$ in Fig. 6 for four solutes and at two temperatures.

Fig. 6 shows that $G_S^{simu}(r, t)$ deviate from the Gaussianity at the most for methane solute, but as the solute size increases $G_S^{simu}(r, t)$ becomes more and more Gaussian in nature. For fullerene, we see practically no difference between $G_S^{simu}(r, t)$ and $G_S^{theo}(r, t)$. This indicates that the dynamical heterogeneity in solute's translation diffusion decreases with increasing the size of the solute. This is consistent with the decrease in the peak height of $\alpha_2(t)$ with increasing solute size. Also, as expected, the deviation of $G_S^{simu}(r, t)$ from the Gaussian behavior is less at 300 K temperature than that at 240 K temperature. In all cases, $G_S^{simu}(r, t)$ crosses $G_S^{theo}(r, t)$ at two *r* values: r_1 and r_2. At the smaller *r* limit ($r < r_1$) the actual displacement of the solute is less than that predicted from the Gaussian $G_S^{theo}(r, t)$. Therefore, the trajectory segment with λ(*t*) less than r_1 is a cage trajectory. On the other hand, beyond $r > r_2$ distance the actual displacement of the solute molecule is larger than the displacement, predicted from $G_S^{theo}(r, t)$[85]. Hence, the trajectory segments, with $\lambda(t) > r_2$, can be termed as jump trajectory. Table 3 lists the numerical values of r_1 and r_2 for different solutes at two temperatures. Fig. 7 presents several examples of jump trajectory segments. Clearly, the present method for identifying the jump event is working as expected.

As the methodology of identifying a jump trajectory is described above, the next step is to count the jump events by counting the peaks of λ(*t*), which cross the cutoff distance r_2. Table 3 summarizes the number of jump events n_J, the jump frequency ν_J (number of jump events per 1 ns), and

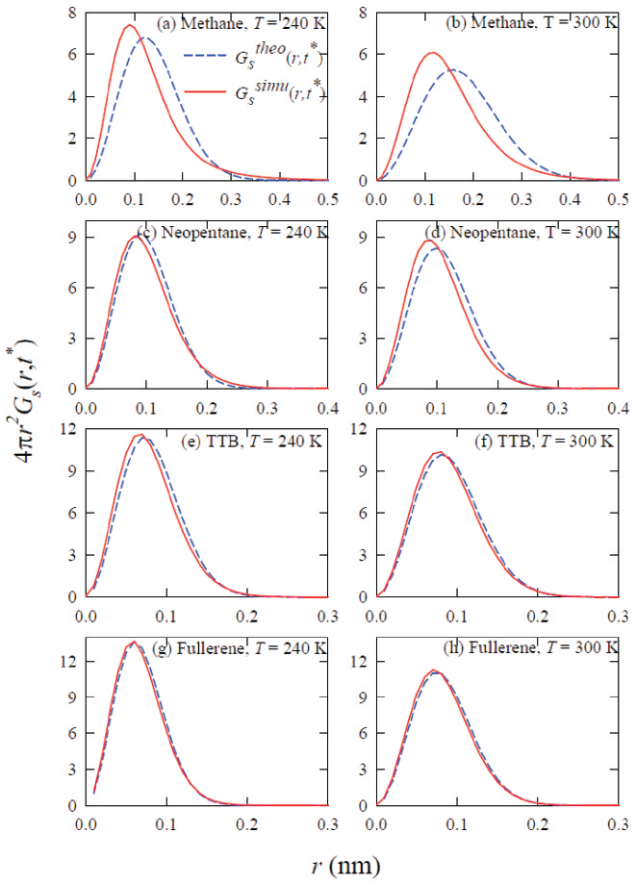

Fig. 6. The self-part of the van Hove correlation functions (solid line) and the corresponding ideal Gaussian distribution ($G_S^{theo}(r, t)$) (dashed line) at time t^* when $\alpha_2(t)$ is maximum. The left hand panels are for T = 240 K, while results for room temperature are presented in right hand panels.

average jump length $\langle\lambda_J\rangle$ (averged over n_J). We see that n_J and ν_J are maximum for methane solute and both the values decrease with increasing solute's size and temperature. This essentially indicates that the importance of jump translation in solute's diffusion increases with decreasing the solute's size and the temperature.

Using ν_J and $\langle\lambda_J\rangle$, listed in Table 3, we now calculate the jump-diffusion coefficient D_J using the following equation[39],

$$D_J = \frac{1}{6}\nu J\langle\lambda^2{}_J\rangle \quad (5)$$

The above equation has been written based on the approximation that the translation jump events stochastically contribute to the jump-diffusion of the solute. The D_J values are listed in Table 4. The percentage contribution of D_J, $\xi_J = (D_J/D)\times 100$, to the overall diffusion coefficient D has also been listed in Table 4. For methane at T = 240 K, ξ_J ~35, which indicates that the jump diffusion of methane contributes approximately 35% to the overall diffusion of methane in supercooled water at 240 K temperatures. For neopentane, the value of ξ_J decreases to ~11. ξ_J further decreases to 0.3 for the larger solute molecule. At the room temperature ξ_J is always less than 1. These observations are the most important results in this study since it provides a quantitative support to the general understanding that the enhancement of the diffusion coefficient on decreasing solute size in the supercooled is due to the gradual dominance of large translational jump.

It was observed earlier that a residual diffusion coeffi-

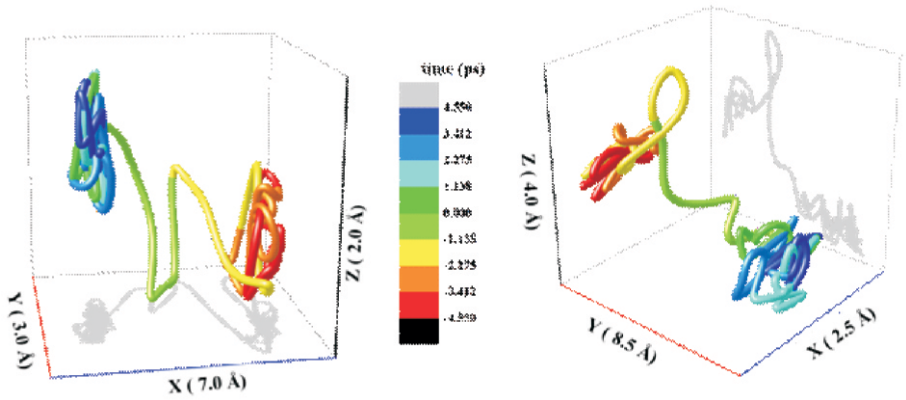

Fig. 7. The jump trajectory segments of methane for the two $\lambda(t)$ values (indicated by vertical red arrows in Fig. 5a) in three-dimensional positional phase space at T = 240 K temperature. The time evolution is color coded.

cient D_{Res} can be calculated by subtracting D_J from the overall diffusion coefficient D using the following equation[39],

$$D_{Res} = D_t - D_{Jump} \quad (6)$$

From the definition, D_{Res} is that component of the overall diffusion, which completely excludes molecular jump translation. Therefore, D_{Res} is primarily the small step diffusion process as in the standard Einstein's Brownian motion. We have calculated D_{Res} for all the solutes and the temperatures and listed the numerical values in Table 4. Table 4 clearly shows that while the D value increases by ~10 times on changing the solute from fullerene to methane (the solute size decreases by ~2.5 times) at 240 K temperature, D_{Res} increases by ~5 times. However, for room temperature, both the D and D_{Res} values increase by ~5 times on the same decrease of the solute size. Therefore, D_{Res}, at 240 K, behaves with solute size very similarly to that at 300 K temperature. This strongly indicates that the excess enhancement of diffusion of a small solute, sometimes termed as 'levitation effect[40], has an overwhelming contribution from the jump-diffusion of the small solute.

Table 4. Different components of diffusion coefficients: total self-diffusion coefficient (D), diffusion coefficient due to jump (D_J), and the residual diffusion coefficient (D_{Res}) of different solute molecules at two different temperatures. Percentage contribution of D_J to D is also listed in the last column

System	T (K)	$D/10^{-6}$ (cm^2/s)	$D/10^{-8}$ (cm^2/s)	$D/10^{-6}$ (cm^2/s)	$\xi_J = (D_J/D)\times100$
Methane	240	1.24	43.0	0.81	34.7
	300	17.4	5.80	17.4	0.34
Neopentane	240	0.46	4.90	0.41	10.7
	300	11.5	1.40	11.5	0.13
TTB	240	0.34	0.10	0.34	0.30
	300	4.51	0.30	4.51	0.07
Fullerene	240	0.15	0.04	0.15	0.27
	300	3.08	0.13	3.08	0.04

4. Conclusion

In conclusion, we have presented a detailed MD simulation study for understanding the hydrophobic solute's size dependence on the self-diffusion coefficient of the solute for both room-temperature and supercooled water. We have reported an increasing diffusion coefficient with decreasing solute's size at both the temperatures. However, the increase of the diffusion is almost double in supercooled water than in water at room temperature. This apparent breakdown of the SE equation for methane and neopentane has been explained by the higher jump-diffusion of the smaller solutes in supercooled water. We have quantitatively estimated the role of translational jump-diffusion in the enhanced diffusion of smaller solutes. By careful consideration of the translational jump trajectories of the solute, we have calculated the jump-only diffusion coefficient D_J. As the solute size is increased, the contribution of D_J to the overall diffusion increases. By subtracting D_J from D, we obtain the residual diffusion coefficient D_{Res}. The effect of enhanced diffusion for the methane solute at 240 K compared to that for fullerene is reduced while we consider D_{Res} of the solute instead of D. This is a clear proof of increasing importance of translational jump-diffusion of the small solute molecule for the observed violation of the SE equation. These new findings can help in elucidating many experimental studies featuring molecular transport properties in more complex chemical and biological environments, where strong diffusion-viscosity decoupling is prevalent.

Acknowledgement

We acknowledge IIT Patna for financial assistance and computational resources. Vikas and Shivam acknowledge IIT Patna for research fellowships. Shakkira acknowledges DST INSPIRE Fellowship (INSPIRE No. IF180090) for funding. We acknowledge SERB Early Career Research Award (File No. ECR/2017/002335) for funding.

References

1. J. Qvist, C. Mattea, E. P. Sunde and B. Halle, *J. Chem. Phys.*, 2012, **136(20)**, 204505.
2. S.-H. Chen, F. Mallamace, C.-Y. Mou, M. Broccio, C. Corsaro, A. Faraone and L. Liu, *Proc. Natl. Acad. Sci. USA*, 2006, **103(35)**, 12974.
3. P. Kumar, *Proc. Natl. Acad. Sci. USA*, 2006, **103(35)**, 12955.
4. A. Dehaoui, B. Issenmann and F. Caupin, *Proc. Natl. Acad. Sci. USA,* 2015, **112(39)**, 12020.
5. M. D. Ediger, C. A. Angell and S. R. Nagel, *J. Phys. Chem.*, 1996, **100(31)**, 13200.
6. G. Heuberger and H. Sillescu, *J. Phys. Chem.*, 1996, **100(37)**, 15255.
7. M. T. Cicerone and M. D. Ediger, *J. Chem. Phys.*, 1996, **104(18)**, 7210.
8. M. T. Cicerone and M. Ediger, *J. Chem. Phys.*, 1995, **103(13)**, 5684.

9. J.-L. Barrat, J.-N. Roux and J.-P. Hansen, *Chem. Phys.*, 1990, **149(1-2)**, 197.
10. J.-N. Roux, J.-L. Barrat and J.-P. Hansen, *J. Phys. Condensed Matter,* 1989, **1(39)**, 7171.
11. G. Wahnström, *Phys. Rev. A,* 1991, **44(6)**, 3752.
12. D. Thirumalai and R. D. Mountain, *Phys. Rev. E,* 1993, **47(1)**, 479.
13. S. Bhattacharyya and B. Bagchi, *J. Chem. Phys.*, 1997, **106(5)**, 1757.
14. S. Bhattacharyya and B. Bagchi, *Phys. Rev. E,* 2000, **61(4)**, 3850.
15. M. D. Ediger, *Annu. Rev. Phys. Chem.,* 2000, **51(1)**, 99.
16. R. Richert, *J. Phys. Condensed Matter,* 2002, **14(23)**, R703.
17. L. J. Kaufman, *Annu. Rev. Phys. Chem.*, 2013, **64**, 177.
18. M. T. Cicerone, Q. Zhong and M. Tyagi, *Phys. Rev. Lett.*, 2014, **113(11)**, 117801.
19. N. Giovambattista, M. G. Mazza, S. V. Buldyrev, F. W. Starr and H. E. Stanley, *J. Phys. Chem. B,* 2004, **108(21)**, 6655.
20. W. Kob, C. Donati, S. J. Plimpton, P. H. Poole and S. C. Glotzer, *Phys. Rev. Lett.*, 1997, **79(15)**, 2827.
21. S. Karmakar, C. Dasgupta and S. Sastry, *Proc. Natl. Acad. Sci. USA,* 2009, **106(10)**, 3675.
22. R. Yamamoto and A. Onuki, *Phys. Rev. E,* 1998, **58(3)**, 3515.
23. H. C. Andersen, *Proc. Natl. Acad. Sci. USA,* 2005, **102(19)**, 6686.
24. V. Dubey, N. Kumar and S. Daschakraborty, *J. Phys. Chem. B,* 2018, **122(30)**, 7569.
25. T. Kawasaki and K. Kim, *Sci. Adv.,* 2017, **3(8)**, e1700399.
26. E. Guillaud, S. Merabia, D. de Ligny and L. Joly, *Phys. Chem. Chem. Phys.*, 2017, **19(3)**, 2124.
27. N. Galamba, *J. Phys. Condensed Matter,* 2016, **29(1)**, 015101.
28. P. Kumar, S. Buldyrev, S. Becker, P. Poole, F. Starr and H. Stanley, *Proc. Natl. Acad. Sci. USA,* 2007, **104(23)**, 9575.
29. A. Furukawa, K. Kim, S. Saito and H. Tanaka, *Phys. Rev. Lett.*, 2009, **102(1)**, 016001.
30. A. D. Parmar, S. Sengupta and S. Sastry, *Phys. Rev. Lett.*, 2017, **119(5)**, 056001.
31. M. Goldstein, *J. Chem. Phys.*, 1969, **51(9)**, 3728.
32. S. Sastry, P. G. Debenedetti and F. H. Stillinger, *Nature,* 1998, **393(6685)**, 554.
33. A. Mukherjee, S. Bhattacharyya and B. Bagchi, *J. Chem. Phys.*, 2002, **116(11)**, 4577.
34. S. Bhattacharyya and B. Bagchi, *Phys. Rev. Lett.*, 2002, **89(2)**, 025504.
35. R. Pastore, A. Coniglio and M. P. Ciamarra, *Soft Matter,* 2014, **10(31)**, 5724.
36. M. P. Ciamarra, R. Pastore and A. Coniglio, *Soft Matter,* 2016, **12(2)**, 358.
37. S. M. Bhattacharyya, B. Bagchi and P. G. Wolynes, *Proc. Natl. Acad. Sci. USA,* 2008, **105(42)**, 16077.
38. S. Indra and S. Daschakraborty, *Chem. Phys. Lett.*, 2017, **685**, 322.
39. S. Dueby, V. Dubey and S. Daschakraborty, arXiv preprint arXiv:1810.03800 2018.
40. M. Sharma and S. Yashonath, *J. Phys. Chem. B,* 2006, **110(34)**, 17207.
41. C. F. Lopez, R. K. Darst and P. J. Rossky, *J. Phys. Chem. B,* 2008, **112(19)**, 5961.
42. M. S. Cheung, A. E. García and J. N. Onuchic, *Proc. Natl. Acad. Sci. USA,* 2002, **99(2)**, 685.
43. M. Munson, S. Balasubramanian, K. G. Fleming, A. D. Nagi, R. O'Brien, J. M. Sturtevant and L. Regan, *Protein Science,* 1996, **5(8)**, 1584.
44. D. Van Der Spoel, E. Lindahl, B. Hess, G. Groenhof, A. E. Mark and H. J. Berendsen, *J. Comp. Chem.,* 2005, **26(16)**, 1701.
45. L. Martínez, R. Andrade, E. G. Birgin and J. M. Martínez, *J. Comp. Chem.,* 2009, **30(13)**, 2157.
46. W. L. Jorgensen, D. S. Maxwell and J. Tirado-Rives, *J. Am. Chem. Soc.,* 1996, **118(45)**, 11225.
47. J. L. Abascal and C. Vega, *J. Chem. Phys.*, 2005, **123(23)**, 234505.
48. B. Chen, M. G. Martin and J. I. Siepmann, *J. Phys. Chem. B,* 1998, **102(14)**, 2578.
49. X. Huang, C. Margulis and B. Berne, *J. Phys. Chem. B,* 2003, **107(42)**, 11742.
50. J. Szala-Bilnik, M. F. Costa Gomes and A. A. Padua, *J. Phys. Chem. C,* 2016, **120(34)**, 19396.
51. S. Nosé, *J. Chem. Phys.*, 1984, **81(1)**, 511.
52. W. G. Hoover, *Phys. Rev. A,* 1985, **31(3)**, 1695.
53. M. Parrinello and A. Rahman, *J. Appl. Phys.*, 1981, **52(12)**, 7182.
54. B. Hess, H. Bekker, H. J. Berendsen and J. G. Fraaije, *J. Comp. Chem.*, 1997, **18(12)**, 1463.
55. H. S. Ashbaugh and M. E. Paulaitis, *J. Am. Chem. Soc.*, 2001, **123(43)**, 10721.
56. S. D. Snow, K. C. Kim, K. J. Moor, S. S. Jang and J.-H. Kim, *Environ. Sci. Technol.*, 2015, **49(4)**, 2147.
57. D. Schlesinger, K. T. Wikfeldt, L. B. Skinner, C. J. Benmore, A. Nilsson and L. G. M. Pettersson, *J. Chem. Phys.*, 2016, **145(8)**, 084503.
58. T. M. Raschke and M. Levitt, *Proc. Natl. Acad. Sci. USA,* 2005, **102(19)**, 6777.
59. A. Godec, J. C. Smith and F. Merzel, *Phys. Rev. Lett.*, 2011, **107(26)**, 267801.

60. U. Schnupf and J. W. Brady, *Phys. Chem. Chem. Phys.*, 2017, **19(19)**, 11851.
61. B. Madan and K. Sharp, *Biophys. Chem.,* 1999, **78(1-2)**, 33.
62. T. Head-Gordon, *Proc. Natl. Acad. Sci. USA,* 1995, **92(18)**, 8308.
63. C. A. Koh, R. P. Wisbey, X. Wu, R. E. Westacott and A. K. Soper, *J. Chem. Phys.*, 2000, **113(15)**, 6390.
64. S. Banerjee, R. S. Singh and B. Bagchi, *J. Chem. Phys.*, 2015, **142(13)**, 04B602_1.
65. R. Sarma and S. Paul *J. Chem. Phys.*, 2012, **136(11)**, 114510.
66. M. Kinoshita, *J. Mol. Liq.*, 2005, **119(1-3)**, 47.
67. M. Kinoshita and F. Hirata, *J. Chem. Phys.*, 1996, **104(21)**, 8807.
68. D. Rapaport and H. Scheraga, *J. Chem. Phys.*, 1982, **86(6)**, 873.
69. N. Galamba, *J. Phys. Chem. B,* 2013, **117(7)**, 2153.
70. E. R. Weeks and D. Weitz, *Chem. Phys.*, 2002, **284(1-2)**, 361.
71. S. Karmakar, C. Dasgupta and S. Sastry, *Phys. Rev. Lett.*, 2016, **116(8)**, 085701.
72. S. Bernini and D. Leporini, *J. Chem. Phys.*, 2016, **144(14)**, 144505.
73. S. Indra and R. Biswas, *J. Phys. Chem. B,* 2016, **120(43)**, 11214.
74. W. Kob and H. C. Andersen, *Phys. Rev. Lett.*, 1994, **73(10)**, 1376.
75. W. Kob and H. C. Andersen, *Phys. Rev. E,* 1995, **51(5)**, 4626.
76. S. Kamath, R. H. Colby, S. K. Kumar and J. Baschnagel, *J. Chem. Phys.*, 2002, **116(3)**, 865.
77. B. Mukherjee, *J. Chem. Phys.*, 2015, **143(5)**, 054503.
78. S. Bhattacharyya, A. Mukherjee and B. Bagchi, *J. Chem. Phys.*, 2002, **117(6)**, 2741.
79. H. Takeuchi, *J. Chem. Phys.*, 1990, **93(3)**, 2062.
80. F. Müller-Plathe, S. C. Rogers and W. F. van Gunsteren, *Chem. Phys. Lett.*, 1992, **199(3-4)**, 237.
81. A. Anil Kumar and S. K. Bhatia, *J. Phys. Chem. B,* 2006, **110(7)**, 3109.
82. S. Acharya, M. K. Nandi, A. Mandal, S. Sarkar and S. M. Bhattacharyya, *J. Phys. Chem. B,* 2015, **119(34)**, 11169.
83. T. E. Raptis, V. E. Raptis and J. Samios, *J. Phys. Chem. B,* 2007, **111(49)**, 13683.
84. T. E. Raptis, V. E. Raptis and J. Samios, *Mol. Phys.*, 2012, **110(11-12)**, 1171.
85. J. C. Araque, S. K. Yadav, M. Shadeck, M. Maroncelli and C. J. Margulis, *J. Phys. Chem. B,* 2015, **119(23)**, 7015.
86. M. S. Shell, P. G. Debenedetti and F. H. Stillinger, *J. Phys. Cond. Matt.,* 2005, **17(49)**, S4035.
87. A. Rahman, *Phys. Rev.*, 1964, **136(2A)**, A405.